Li Ming (Orcid ID: 0000-0003-1492-4127)
Glibert Patricia (Orcid ID: 0000-0001-5690-1674)

# Seasonal life strategy of *Prorocentrum minimum* in Chesapeake Bay, USA: Validation of the role of physical transport using a coupled physical-biogeochemical-harmful algal bloom model

Ming Li* (ORCID ID: 0000-0003-1492-4127, mingli@umces.edu),

Fan Zhang (ORCID ID: 0000-0002-9637-0529, fzhang@umces.edu),

Patricia M. Glibert (ORCID ID: 0000-0001-5690-1674, glibert@umces.edu)

University of Maryland Center for Environmental Science

Horn Point Laboratory

PO Box 775, Cambridge, Maryland 21613, U.S.A.

Submitted to *Limnology and Oceanography*

*Correspondence to: Ming Li, Horn Point Lab, University of Maryland Center for Environmental Science, Cambridge, Maryland 21613, U.S.A. Email: mingli@umces.edu. Fan Zhang, Horn Point Lab, University of Maryland Center for Environmental Science, Cambridge, Maryland 21613, U.S.A. Email: fzhang@umces.edu.

**Running head:** Life strategy of *Prorocentrum minimum*

**Key words:** harmful algal blooms, *Prorocentrum minimum*, life cycle strategy, physical

transport, estuarine circulation

**Abstract**

Over 40 years ago, it was suggested that *Prorocentrum minimum* in Chesapeake Bay has a seasonal life strategy that depends on the physical transport by estuarine circulation, bringing cells from lower bay to the mid bay in spring when they bloom. In this study, a validated hydrodynamic-biogeochemical model is used to simulate the annual cycles of *P. minimum* in Chesapeake Bay and track its life history over multiple years. The model reproduces the observed seasonal progression of *P. minimum* without a seed population. Four life stages of *P. minimum* are faithfully produced in the model: (1) in winter, overwintering populations from the previous bloom are distributed throughout the water column in the lower bay; (2) in late winter/early spring, cells are transported upstream by the landward bottom flows; (3) in May, *P. minimum* develops a bloom in the mid-bay; (4) in late summer/fall, decaying *P. minimum* populations are transported downstream by the seaward surface flows. Particle tracking shows that it takes about 3-4 months for the overwintering cells to travel from the lower bay to the mid-bay, but about 6 months for the decaying cells to travel from the mid-bay to the lower bay, as the estuarine circulation is far stronger during the high runoff months of January-May than during the low runoff months of June-December. With the peak growth rate around 20$^{o}$C, May provides an optimal window of growth opportunity for *P. minimum* as phytoplankton assemblage transitions from winter-spring diatoms to summer dinoflagellates in a seasonal succession.

## Introduction

In a study published over 40 years ago, Tyler and Seliger (1978) proposed a novel mechanism for the life cycle strategy of the red tide dinoflagellate *Prorocentrum minimum* in Chesapeake Bay. During January and February they observed significant concentrations of *P. minimum* cells below the photic zone in the lower bay, at a distance of 200 km downstream of the region where blooms typically appear later in the year. Based on several bay-wide ship surveys (January, February, March, May, August, November-December) over a span of two years (Fig. 1), they hypothesized that *P. minimum* in surface outflowing waters at the mouth of the bay was recruited in late winter into more dense inflowing coastal waters and then transported northward to reach its bloom area in the upper part of the mid-bay by late spring. They further hypothesized that *P. minimum* was not introduced into the bay from surface waters of the Atlantic Ocean, but rather resulted from the decaying *P. minimum* bloom that was transported seaward by the estuarine outflow from the previous year's bloom. This hypothesis of Tyler and Seliger (1978, TS78 hereafter) is remarkable because it suggests a self-sustaining life strategy of an estuarine HAB species that does not require a remote source of seed populations nor does it involve a life stage as cysts buried under the sea bed. It also begs for a reexamination in light of recent laboratory, field and modeling studies of *Prorocentrum* blooms and the recognition that planktonic *Prorocentrum* species have proliferated in estuarine and coastal waters worldwide over the past few decades, especially in relation to eutrophication (Heil et al. 2005; Glibert et al. 2008, 2012; J. Li et al. 2015; M. Li et al. 2020; Zhang et al. 2021).

Many HAB species have relatively modest growth rates when compared with other phytoplankton species. It is intriguing how slow-growing HAB species out-compete other

species to develop blooms, and life cycle strategies have long been suspected of giving some HAB species a competitive advantage (Stolte and Garces 2006; Hense 2010; Azanza et al. 2018). For example, transitions between resting and vegetative phases in the dinoflagellates *Alexandrium fundyense* and *Pyrodinium bahamense* were found to be responsible for initiating or terminating blooms (e.g., Anderson 1998; Garcés et al. 2002; Anderson and Rengefors 2006). Resting cells from previous blooms settle on the sea bed, where they accumulate and form a so-called seed bank. Seed banks and blooms are not necessarily in the same geographic location due to transport of the different life cycle stages by ocean currents; offshore germinating cells may be advected onshore initiating a coastal bloom (e.g., McGillicuddy et al. 2003), while an offshore HAB may be generated by germinating cells originating at a coastal seed bank (Donaghay and Osborn 1997). Other HAB life cycle strategies include *Pseudo-nitzschia* diatom species undergoing sexual reproduction (Lelong et al. 2012; Montresor et al. 2016) and cyanobacteria forming akinetes as a resting stage (Huber 1984; Suikkanen et al. 2010). All these life cycle strategies involve biological processes, which stand in contrast to the above *P. minimum* life strategy that relies entirely on physical processes.

The TS78-reported bimonthly surveys of *P. minimum* and currents in Chesapeake Bay made a strong case for the physical transport mechanism as a life strategy, but a direct test of this mechanism has been lacking. Such a test requires tracking *P. minimum* cells over a complete life cycle as they move between the bloom region in the upper part of the mid-bay and overwintering site in the lower bay. Although chemical and genomic markers have been used to track marine species such as oyster larvae (Gancel et al. 2019; Houston et al. 2020), it has been impractical to carry out the detailed surveys of *P. minimum* over several years that would be necessary for such

an empirical test. On the other hand, a well validated numerical model can track movements of HAB cells in space and over time. In this paper we apply a validated coupled hydrodynamic-biogeochemical model, ROMS-RCA-*Prorocentrum* (Zhang et al. 2021), to study the life cycle strategy of *P. minimum* in Chesapeake Bay. Specifically, we run the model in a 'perpetual' mode by repeating annual forcing over a number of years thereby testing if the *P. minimum* life cycle is repeated and sustained every year. This approach has been widely used in climate modeling studies to examine the stability of a seasonal/annual cycle in a climate system under different climatic forcing conditions (e.g., Zwiers and Boer 1987; Brossier et al. 2011).

## Methods

*ROMS-RCA*-Prorocentrum *model*

The ROMS-RCA-*Prorocentrum* model has three components (Zhang et al. 2021). The 3D hydrodynamic model is based on the Regional Ocean Modeling System (ROMS) (Shchepetkin and McWilliams 2005; Haidvogel et al. 2008), and the biogeochemical model is based on the Row Column Aesop (RCA) structure (DiToro 2001; Isleib et al. 2007). The *Prorocentrum* model uses the rhomboid approach in which the individual HAB taxa is characterized against a background of other functional groups (Zhang et al. 2021).

The ROMS hydrodynamic model domain covers the Chesapeake Bay and its adjacent shelf, and has been validated against a wide variety of observational data (M. Li et al. 2005; Zhong and Li 2006; M. Li et al. 2006; Xie and Li 2018; Xie et al. 2018). The model has 80 x 120 grid points in the horizontal directions and 20 vertical levels. ROMS is forced by freshwater discharge at river heads, water levels at the open boundary, and heat and momentum flux across

the sea surface. The freshwater input is prescribed for the 8 major tributaries of Chesapeake Bay, based on measurements at US Geological Survey gaging stations. At the offshore boundary, the tidal component is provided by TPXO7 (Egbert and Erofeeva 2002), and non-tidal component is extracted from daily sea level measured at Duck, North Carolina, by National Oceanic and Atmospheric Administration (NOAA). The air-sea heat flux and momentum flux are calculated using the North America Regional Reanalysis (NARR) data.

The RCA biogeochemical model is coupled to the ROMS hydrodynamic model in an offline mode. Hourly averages of temperature, salinity, and transport terms from ROMS are used to drive the biogeochemical variables in RCA. The RCA has a water-column component (Isleib et al. 2007; Zhang and Li 2010) and a two-layer sediment diagenesis model (DiToro et al. 2001; Brady et al. 2013). The water-column model includes state variables representing dissolved inorganic nitrogen (DIN), dissolved inorganic phosphorus (DIP), and silicate (Si), particulate and dissolved organic N and P, and dissolved $O_2$. The phytoplankton module includes two generic algal assemblages and one species: one winter group (optimum temperature ~10$^o$C), one summer group (optimum temperature ~25$^o$C), and *P. minimum*. For the *P. minimum* model, the growth rate depends on temperature, light and nutrient concentrations, while the mortality terms include both grazing and respiration, and the model parameters have been calibrated according to published physiological experiments on *P. minimum* and numerical sensitivity-analysis experiments (Zhang et al. 2021). At the heads of the tributaries, the nutrient concentration and two phytoplankton assemblages are prescribed based on Chesapeake Bay Program data and *P. minimum* concentration is set to zero as there is no evidence suggesting that external input is a significant source of *P. minimum* in the Bay. At the offshore boundary, nutrient concentrations

on the shelf are acquired from the World Ocean Atlas and Filippino et al. (2011). ROMS-RCA was previously validated in several modeling studies (Testa et al. 2014; M. Li et al. 2016; Testa et al. 2017; Ni et al. 2020).

A detailed validation of ROMS-RCA-*Prorocentrum* in Chesapeake Bay was presented in Zhang et al. (2021), showing good skills in predicting DIN as nitrate plus nitrite ($NO_3^-$+$NO_2^-$) and ammonium ($NH_4^+$), DIP as phosphate ($PO_4^{3-}$), chlorophyll *a*, and *P. minimum* cell density at a number of monitoring stations. The validated model not only predicted the seasonal timing and location of *P. minimum* blooms but also captured the observed interannual variations in the magnitude and distributions of *P. minimum* blooms.

In the ROMS-RCA-*Prorocentrum* model (Zhang et al. 2021), the growth rate of *P. minimum* is written as

$$G = G_T * G_{par} * G_N. \quad (1)$$

The specific growth rate $G_T$ is given by

$$G_T = \begin{cases} G_p e^{-\beta_1 (T-T_{opt})^2} & (T \le T_{opt}) \\ G_p e^{-\beta_2 (T-T_{opt})^2} & (T \ge T_{opt}) \end{cases} \quad (2)$$

where $G_p$ is the maximum growth rate, $T_{opt}$ is the optimal temperature for the maximum growth, and $\beta_1$ and $\beta_2$ are shape factors characterizing the window of optimal growth. The effect of light (as photosynthetically active radiation, PAR) availability on *P. minimum* growth ($G_{par}$) is parameterized by

$$G_{par} = \frac{\alpha * PAR}{\sqrt{{G_T}^2 + (\alpha * PAR)^2}} \quad (3)$$

in which $\alpha$ is the slope of the P-I curve (in unit of $ly^{-1}$). The effect of nitrogen limitation on *P. minimum* growth is parameterized by

$$G_{DIN} = \frac{DIN}{DIN+K_{mn}}, \quad (4)$$

and the effect of phosphorous limitation is parameterized by

$$G_{DIP} = \frac{DIP}{DIP+K_{mp}} \quad (5)$$

where $K_{mn}$ and $K_{mp}$ are the half saturation constants for DIN and DIP, respectively. The net effect of nutrient limitation on *P. minimum* growth is given by

$$G_N = min(G_{DIN},\ G_{DIP}). \quad (6)$$

These terms are herein analyzed to discern mechanisms regulating the timing and location of *P. minimum* blooms.

*Perpetual run configuration*

To configure the perpetual model runs, we selected year 2007 for the annual forcing as the river discharge in that year was close to the long-term average. The ROMS model was initialized with climatological temperature and salinity and was run for a spin-up period of 3 years. The outputs of this spin-up run were used to set the initial conditions for the hydrodynamic model in the perpetual run. The nutrients and phytoplankton assemblages in RCA model were initialized on January 1, 2007 with observational data from Chesapeake Bay Program. Observations of *P. minimum* were limited during winter with only 4 data records in the main stem of the Bay. As such, the initial condition for *P. minimum* was constructed based on both the observation in January 2007 and the bay wide survey from TS78. The ROMS-RCA-*Prorocentrum* model was forced with the same annual forcing and ran for several years until repeating annual life cycles were established.

*Particle transport model*

To further clarify the physical transport mechanism, the Larval TRANSport Lagrangian model (LTRANS) was used to track the trajectories of neutrally buoyant particles (North et al. 2008). LTRANS simulates particle advection by the velocity fields and incorporates a random displacement model to simulate particle random walk due to turbulent diffusion. To test the first half of *P. minimum* life history, 12 particles were released in the model at a lower-bay location on 1 January and tracked until the end of June. To test the second half of *P. minimum* life history, 20 particles were released at a mid-bay location on 1 July and tracked until the end of December. Both sets of particles were initially placed at 1 m intervals from the surface to the bottom at their respective locations.

## Results

*Repeating annual cycles*

The time series of surface water *P. minimum* cell concentrations at 8 stations along the center axis of Chesapeake Bay show repeating annual cycles (Fig. 2). There are differences in cell density between the first two years as the model adjusts to the annual forcing and the influence of the initial condition fades. However, the *P. minimum* time series show repeating annual cycles at all the stations from years 3. The annual cycles show a pattern of low cell concentration between January and April, an initiation of a bloom in the beginning of May, reaching a peak in mid- to late May, and then termination by mid- to late June. After that, the cell concentration drops to low levels during the rest of the year. A late-spring *P. minimum* bloom is sustained every year, completely independent of the initial seed concentration.

Differences in the bloom magnitude were predicted by the model among the stations (Fig. 2). The predicted peak cell concentration is about 1 x $10^6$ cell $L^{-1}$ at the two upper bay stations (CB 2.2 and CB 3.1) as well as at the two lower bay stations (CB 5.2 and CB 6.1). In comparison, the predicted peak cell concentration reaches nearly 2 x $10^6$ cell $L^{-1}$ at the four mid-bay stations (CB 3.3C, CB 4.1C, CB 4.2C, CB 4.3C), indicating that the most intense *P. minimum* blooms develop in this mid-bay region.

*Transport pathways*

Next, the along-channel distributions of monthly mean *P. minimum* cell concentration were compared with the monthly mean residual circulation (Fig. 3). During January, most *P. minimum* cells are located on the shallow lower bay and are present at all depths, as strong turbulent mixing disperses cells throughout the weakly stratified water column (Fig. 3a). The estuarine return flows (~0.05-0.15 m $s^{-1}$) in the bottom layer transport the cells landward such that a plume of low cell concentration water spills into the deep mid-bay, in agreement with the cell distribution reported in TS78's January survey (compare Figs. 1b and 3a). In February, the cell density in the lower bay decreases but the plume of low cell concentration water penetrates further upstream (compare Fig. 3b with Fig. 1c). The *P. minimum* cell distribution in March covers a similar latitudinal extent as in February, but reaches higher in the water column (up to 10 m depth) as mixing diffuses the cells upwards (M. Li et al. 2005; M. Li and Zhong 2009; Y. Li and M. Li 2011; M. Li et al. 2016). By April low cell concentrations appear throughout the water column.

A model-predicted *P. minimum* bloom develops in May, with the highest concentration in the surface waters of the mid-bay, at a distance of 150-250 km from the estuary's mouth (Fig. 3e). This was also shown clearly in TS78's field survey in May (Fig. 1d). This bloom weakens considerably in June and July (Figs. 3f and 3g). By August, the cells are mostly confined to a region about 250 km from the estuary's mouth (Fig. 3h), as shown in TS78's survey in August (Fig. 1e). Over the next few months, a plume of low *P. minimum* cell density is advected seaward by the surface outflow, with its front edge reaching 170-150 km from the mouth in September and October (Figs. 3i and 3j), and at the 120 km mark in November (Fig. 3k), and at the 70 km mark in the lower bay in December (Fig. 3l).

It is of note that the transport of *P. minimum* cells from the lower bay to the mid-bay (200-250 km) takes about 3-4 months (from January to May), but the transport of *P. minimum* cells from the upper part of the mid-bay to the lower bay takes about 6 months (from July to December). This difference can be explained by the seasonal difference in the estuarine circulation strength. The river flow is much higher (up to 6000 $m^3 s^{-1}$) between January and May, but much lower during the summer and fall (down to 300-400 $m^3 s^{-1}$) (Fig. 4a). Consequently, the residual estuarine circulation is much stronger during the winter-spring months, with the landward flow in the lower layer averaging ~0.1 $m\ s^{-1}$ at the mid-bay location that is 150 km from the bay's mouth (Fig. 4b). In comparison, the estuarine circulation is much weaker between July and December, with the seaward flow in the upper layer averaging to ~0.05 $m\ s^{-1}$.

The particle tracking model, LTRANS, further demonstrated how the estuarine return flow transports overwintering populations to the mid-bay to fuel a bloom during winter-spring

and how the estuarine outflow transports decaying cells to the lower bay during summer and fall (Fig. 5). For the test representing the first half of *P. minimum* life history, particles were released at a lower bay location on 1 January and tracked until the end of June (Figs. 5a-5f). Some particles in the surface layer are exported out to the shelf while other particles are advected landward by the estuarine return flow, reaching 38 $^{o}$N by 1 March and 38.5 $^{o}$N by 1 May. The later location is the mid-bay region where *P. minimum* bloom typically occurs. For the test representing the second half of *P. minimum* life history, particles were also released at a mid-bay location on 1 July and tracked until the end of December (Figs. 5g-5l). A few particles move upstream, other particles move progressively seaward. By November and December, some particles reach the lower bay and are located in the lower layer. The two particle tracking calculations confirm the landward transport pathway between January and May and the seaward transport pathway over the summer and fall.

*A window of growth opportunity for blooms*

To understand why favorable conditions for *P. minimum* occur in the mid-bay in May, model-predicted surface distributions of DIN and DIP, PAR (at 2 m depth), *P. minimum* cell concentration, DIN limitation, DIP limitation, light limitation, and *P. minimum* growth rate were examined. High river flows during January and April deliver high concentrations of DIN and DIP to the upper and middle parts of the estuary (Figs. 6a-b) whereas at this time of year PAR is low in the upper bay due to incoming riverine sediment (Fig. 6c). The region between 38.5 and 39.2 $^{o}$N represents the overlap area where both nutrient concentrations and the light field are favorable for *P. minimum* growth.

DIN is not limiting *P. minimum* growth in most parts of Chesapeake Bay at this time of year, as $G_{DIN}$ approaches 1 (Fig. 6e). On the other hand, $G_{DIP}$ is in the range of 0.8 -1 in the upper Bay but drops dramatically south of 38.5 $^{o}$N (Fig. 6f). Hence nutrient limitation on *P. minimum* growth is mainly determined by P limitation. Values of $Gpar$ are low north of 39 $^{o}$N but approach 1 south of this latitude (Fig. 6g). The actual growth rate of *P. minimum* during May is highest in the region between 37.8 and 39 $^{o}$N (Fig. 6h), which corresponds reasonably well to the region with highest cell density (Fig. 6d), although a precise correspondence is not expected as the biomass also depends on grazing and respiration and is affected by physical transport. Therefore, the *P. minimum* bloom develops in the mid-bay region due to the optimal light and nutrient conditions there.

The month of May also provides an optimal window of growth opportunity for *P. minimum* as water temperature in May matches the optimal temperature for *P. minimum* growth at ~20$^{o}$C (Fig. 7a). In comparison, the winter-spring diatom group is parameterized in the model with optimum temperature for growth of ~10$^{o}$C and the summer dinoflagellate group is parameterized in the model with an optimum temperature for growth of ~25$^{o}$C. A comparison of the specific growth rates $G_T$ for the three phytoplankton groups shows the diatom's domination between December to mid-April and the summer assemblage's domination between June and October. The two windows of opportunity for *P. minimum* growth are 1) a late spring period from mid-April to end of May and 2) a late fall period from late October to end of November (Fig. 7b). The actual growth rates of these phytoplankton species also depend on nutrient concentration and light availability. At the mid-bay station 4.1C, the diatom group reaches a peak growth rate of over 1 mg C $L^{-1}$ $d^{-1}$ in March and April, *P. minimum* reaches a peak growth

rate of about 1 mg C $L^{-1}$ $d^{-1}$ in May, and the summer assemblage reaches a peak growth rate of about 2 mg C $L^{-1}$ $d^{-1}$ in June to August (Fig. 7c). The phytoplankton biomass shows a diatom maximum of 1 mg C $L^{-1}$ during March and April, a *P. minimum* maximum of 0.5 mg C $L^{-1}$ in May, and a summer assemblage maximum of over 1 mg C $L^{-1}$ in summer and early fall (Fig. 7d). Therefore, due to its window of growth opportunity around ~20°C, *P. minimum* manages to develop a bloom in late spring as the phytoplankton seasonal succession transitions from the winter-spring diatom group to the summer dinoflagellate group.

*Sensitivity to model parameters*

The above results were obtained from the model run (control run) using a set of parameter values determined according to published physiological experiments on *P. minimum* (summarized in Zhang et al. 2021). There are uncertainties in estimating some parameters such as the maximum growth rate $G_p$ and the shape factors $\beta_1$ and $\beta_2$ characterizing the window of optimal growth. We have conducted 4 additional sensitivity-analysis model runs with $G_p$, $\beta_1$ and $\beta_2$ increased or decreased by 20% (Fig. 8). Reducing $G_p$ by 20% substantially suppresses the bloom (Fig. 8b). In contrast, increasing it by 20% enhances the peak bloom size by ~30% and also lengthens the bloom duration (Fig. 8c). When $\beta_1$ and $\beta_2$ decrease by 20%, *P. minimum* has a longer window of opportunity to grow and its bloom lasts longer (Fig. 8d). When $\beta_1$ and $\beta_2$ increase by 20%, the window of growth opportunity is shortened, resulting in a shorter bloom duration and a smaller bloom size (Fig. 8e). Overall, the seasonal progression of the *P. minimum* bloom in the sensitivity-analysis model runs is similar to that shown in Fig. 3, despite that the bloom size and duration are sensitive to changes in these parameters.

## Discussion

The perpetual model simulations using a 3D coupled hydrodynamic-biogeochemical model has confirmed the life strategy of *P. minimum* proposed by Tyler and Seliger (1978). In summary, *P. minimum* has four life stages: (1) in winter, overwintering populations from the previous bloom are mixed throughout the water column in the lower bay due to strong turbulent mixing; (2) in late winter/early spring, cells are transported upstream by the landward bottom flows with a travel time of about 3-4 months since the estuarine circulation is strong during the high runoff months of January to April; (3) in May, *P. minimum* develops a bloom in the upper part of the mid-bay due to optimal growth conditions there; and (4) in late summer/fall, decaying *P. minimum* populations are transported downstream by the seaward surface flows from the mid- to the lower bay by the estuarine outflow in the surface layer, taking about 6 months since the estuarine circulation is much weaker during the low runoff seasons of summer and fall (Fig. 9). During this annual cycle *P. minimum* exhibits two distinct phases in terms of growth: a "rapid growth phase" between late April and early July when cells are actively growing and a "slow growth phase" between August and April in the follow year when post-bloom cells first move towards the mouth of the Bay and then return in the bottom layer (Figs. 3 and 7). During the latter period, both the growth rate and mortality rate are very low. This study has demonstrated the feasibility of a unique self-sustaining life strategy of a HAB species that relies entirely on the physical transport mechanism. It does not require a remote source of seed populations nor involves a life stage as cysts buried under the sea bed.

It is also interesting to note that *P. minimum* takes advantage of an optimal growth window in May as the phytoplankton assemblage in Chesapeake Bay makes a transition from the

March-April spring bloom of diatoms to the fast-growing summer assemblage in a seasonal succession. *P. minimum* typically only constitutes 20-30% of the total phytoplankton biomass in Chesapeake Bay (Adolf et al. 2006). Moreover, its specific growth rate is lower than that of both the winter-spring diatoms and the summer dinoflagellates (Testa et al. 2014). It appears that *P. minimum* squeezes a bloom in between the blooms of the two dominant phytoplankton groups because its optimal temperature for growth (~20$^{o}$C) is greater than that of the winter-spring diatoms, but less than that of the summer assemblage. The location of the bloom in the upper part of the mid-bay points to *P. minimum*'s exploitation of optimal conditions of nutrient concentration and light field.

In a subsequent paper, Tyler and Seliger (1981) found that the growth rate of *P. minimum* depends on both temperature and salinity. In particular, the growth rate increased with salinity in low temperature waters, thus restricting the over-wintering populations to the high-salinity lower bay. This salinity-enhanced growth rate appears to be at odds with the laboratory experiments of Grzebyk and Berland (1996) which showed a moderately higher growth rate in an intermediate range of salinities. Tyler and Seliger (1981) also suggested an optimal temperature growth of *P. minimum* around ~25 °C, but recent field observations of *P. minimum* in Chesapeake Bay clearly showed highest bloom density at a temperature range between 13 and 25 °C (Tango et al. 2005). Zhang et al. (2021) compared the model simulations with or without salinity dependence in the specific growth of *P. minimum* but found little differences in the model results. We also conducted a perpetual model run with the salinity dependence and found a similar result. Therefore, the physical transport mechanism does not require a salinity-enhanced growth rate to sustain the overwintering populations in the high salinity lower bay.

Model-sensitivity analysis showed that the four seasonal life stages of *P. minimum* remain the same, although the bloom size and bloom duration are sensitive to changes in the maximum growth rate and the shape parameters characterizing the optimal window of growth. Zhang et al. (2021) reported additional model-sensitivity analysis and found that the model-predicted bloom size was particularly sensitive to the half saturation constant for phosphorous uptake. Despite the uncertainty in determining these physiological parameters from laboratory experiments and the model's sensitivity to these parameters, it should be noted that the model was able to capture the large interannual variability of the *P. minimum* blooms in a decadal hindcast simulation using the same set of parameter values (Zhang et al. 2021).

In all, the insight from over 40 years ago, based on multi-year bay-wide field surveys (Tyler and Seliger 1978), has been confirmed using a contemporary 3D coupled hydrodynamic-biogeochemical model parameterized for *P. minimum*. The model was run using average flow conditions and captured the peak in bloom development in May in the mid-to-upper parts of the estuary. The model also showed the potential window of opportunity for a fall bloom, which did not develop under average conditions, but with shifts in flows, storms and temperature, such blooms may occur and are, in fact, observed in some years (Tango et al. 2005; J. Li et al. 2015; M. Li et al. 2020). For example, a fall bloom developed in late fall in 2006, as storms injected nutrients and cells into the surface euphotic layer, leading to a second peak in the growth rate of *P. minimum* (Zhang et al. 2021).

Globally, *P. minimum* blooms are expanding in coastal and estuarine waters, and their association with increasing eutrophication has been documented (Glibert et al. 2008, 2012 and references therein). As climate changes, and associated increasing temperatures, altered stratification and density gradients, as well as altered propensity and intensity of precipitation events, the window of opportunity for *P. minimum* may change in Chesapeake Bay as well as elsewhere (M. Li et al. 2020). Springs in Chesapeake Bay are expected to become wetter, and it is projected that this will increase N loads–even in the absence of increases in land-based applications; an increase in N flux down the Susquehanna River (the major tributary of Chesapeake Bay) of 17% by 2030 and 65% by 2095 is expected from flow changes alone (Howarth 2008). Based on climate downscaling models for the Chesapeake Bay region, projected for the years 2041-2070, DIN loads will not only increase in spring, but DIN:DIP will also increase substantially, increasing the potential habitat for species such as *P. minimum* (Glibert 2020; M. Li et al. 2020). Understanding the role of physical transport in conjunction with habitat changes through modeling gives new opportunities to explore the vulnerability for blooms in the future, not only in the bay, but in coastal and estuarine regions worldwide where physical models are available.

**Acknowledgement**

We thank the two reviewers for their helpful comments. This work is funded by the National Oceanic and Atmospheric Administration National Centers for Coastal Ocean Science Competitive Research Program under award NA17NOS4780180 to UMCES. This is ECOHAB contribution number ECO996 and contribution number 6032 from the University of Maryland Center for Environmental Science.

Model output is available at https://doi.org/10.5281/zenodo.3525203.

**Conflict of Interest**

None declared.

**Arthur Contributions:**

ML and PMG conceived the study. FZ conducted the numerical model simulations. ML and FZ conducted the analysis of model results. ML wrote the original draft, and PMG reviewed and edited the draft.

**References:**

Adolf, J.E., C.L. Yeager, W.D. Miller, M.E. Mallonee, and L.W. Harding, Jr. 2006. Environmental forcing of phytoplankton floral composition, biomass, and primary productivity in Chesapeake Bay, USA. Est. Coast. Shelf Sci. **67**: 108–122.

Anderson, D.M., 1998. Physiology and bloom dynamics of toxic *Alexandrium* species, with emphasis on life cycle transitions. In D.M. Anderson, A.D. Cembella, G.M. Hallegraeff [eds.], Physiological Ecology of Harmful Algal Blooms — NATO ASI Series, G41. Springer-Verlag, Berlin, pp. 29–48.

Anderson, D.M. and K. Rengefors. 2006. Community assembly and seasonal succession of marine dinoflagellates in a temperate estuary: the importance of life cycle events. Limnol. Oceanogr. **51**: 860–873.

Azanza, R.V., M.L. Brosnahan, D.M. Anderson, I. Hense, and M. Montresor. 2018. The role of life cycle characteristics in harmful algal bloom dynamics. In Glibert, P.M., E. Berdalet,

M.A. Burford, G.C. Pitcher and M. Zhou [eds.], Global ecology and oceanography of harmful algal blooms. Ecological Studies 232, Springer Nature, pp. 133-161. doi.org/10.1007/978-3-319-70069-4_8

Brady, D.C., J.M. Testa, D.M. Di Toro, W.R. Boynton, and W.M. Kemp, W. M. 2013. Sediment flux modeling: Calibration and application for coastal systems. Est. Coast. Shelf Sci**. 117**: 107-124. https://doi.org/10.1016/j.ecss.2012.11.003

Brossier, C. L., K. Béranger, C. Deltel, and P. Drobinski. 2011. The Mediterranean response to different space–time resolution atmospheric forcings using perpetual mode sensitivity simulations. Ocean Model. **36**(1-2): 1-25.

Di Toro, D. M. (2001), Sediment flux modeling. Wiley-Interscience, New York. 624 pp.

Donaghay, P.L. and T.R. Osborn. 1997. Toward a theory of biological–physical control of harmful algal bloom dynamics and impacts. Limnol. Oceanogr. **42/5**: 1283–1296.

Egbert, G. D and S.Y. Erofeeva. 2002. Efficient inverse modeling of barotropic ocean tides. J. Atmos. Ocean. Technol. **19**(2): 183-204.

Filippino, K. C., M.R. Mulholland, and P.W. Bernhardt. 2011. Nitrogen uptake and primary productivity rates in the Mid-Atlantic Bight (MAB). Est. Coast. Shelf Sci. **91**(1): 13-23.

Gancel, H. N., R.H. Carmichael, K. Park, J.W. Krause and S. Rikard. 2019. Field mark-recapture of calcein-stained larval oysters (*Crassostrea virginica*) in a freshwater-dominated estuary. Est. Coasts **42**(6): 1558–1569. doi: 10.1007/s12237-019-00582-6.

Garcés, E., M. Masó, and J. Camp. 2002. Role of temporary cysts in the population dynamics of *Alexandrium taylori* (Dinophyceae). J. Plankt. Res. **24**: 681–686.

Glibert, P.M. 2020. Harmful algae at the complex nexus of eutrophication and climate change. Harmful Algae **91**: 101583. doi:10.1016/j.hal.2019.03.001.

Glibert, P. M., E. Mayorga, S. Seitzinger. 2008. *Prorocentrum minimum* tracks anthropogenic nitrogen and phosphorus inputs on a global basis: application of spatially explicit nutrient export models. Harmful Algae **8**(1): 33-38.

Glibert, P.M., J.M. Burkholder, and T.M. Kana. 2012. Recent insights about relationships between nutrient availability, forms, and stoichiometry, and the distribution, ecophysiology, and food web effects of pelagic and benthic *Prorocentrum* species. Harmful Algae **14**: 231–259.

Grzebyk, D. and B. Berland. 1996). Influences of temperature, salinity and irradiance on growth of *Prorocentrum minimum* (Dinophyceae) from the Mediterranean Sea. J. Plankt. Res. **18**(10): 1837-1849.

Haidvogel, D. B., and others. 2008. Ocean forecasting in terrain-following coordinates: Formulation and skill assessment of the Regional Ocean Modeling System. J. Computat. Phys. **227**(7): 3595-3624.

Heil, C. A. 2005. Influence of humic, fulvic and hydrophilic acids on the growth, photosynthesis and respiration of the dinoflagellate *Prorocentrum minimum* (Pavillard) Schiller. Harmful Algae **4**(3): 603-618.

Hense, I. 2010. Approaches to model the life cycle of harmful algae. J. Mar. Sys. **83**: 108-114. doi:10.1016/j.jmarsys.2010.02.014

Houston, R.D., T.P. Bean, D.J. Macqueen, M.K. Gundappa et al. 2020. Harnessing genomics to fast-track genetic improvement in aquaculture. Nat. Rev. Genet. **21**: 389-409. doi.org/10.1038/s41576-020-0227- y.

Howarth, R. W. 2008. Coastal nitrogen pollution: a review of sources and trends globally and regionally. Harmful Algae **8**:14-20.

Huber, A.L. 1984 *Nodularia* (Cyanobacteriaceae) akinetes in the sediments of the Peel-Harvey Estuary, Western Australia: potential inoculum source for *Nodularia* blooms. Appl. Envir. Microbiol. **47**(2):234–238.

Isleib, R. R., J.J. Fitzpatrick and J. Mueller. 2007. The development of a nitrogen control plan for a highly urbanized tidal embayment. Proceed. Wat. Environ. Fed. **2007**(5), 296-320.

Lelong A, H. Hégaret, P. Soudant and S.P. Bates. 2012. *Pseudo-nitzschia* (Bacillariophyceae) species domoic acid and amnesic shellfish poisoning: revisiting previous paradigms. Phycologia **51**:168–216.

Li, J., P.M. Glibert and Y. Gao. 2015. Temporal and spatial changes in Chesapeake Bay water quality and relationships to *Prorocentrum minimum, Karlodinium veneficum*, and CyanoHAB events, 1991–2008. Harmful Algae **42:** 1-14.

Li, M., L. Zhong, and W.C. Boicourt. 2005. Simulations of Chesapeake Bay estuary: Sensitivity to turbulence mixing parameterizations and comparison with observations. J. Geophys. Res.: Oceans **110**(C12). doi:10.1029/2004JC002585.

Li, M., L. Zhong, W.C. Boicourt, S. Zhang, and D.L. Zhang. 2006. Hurricane‐induced storm surges, currents and destratification in a semi‐enclosed bay. Geophys. Res. Lett., **33**(2). doi:10.1029/2005GL024992.

Li, M. and L. Zhong. 2009. Flood-ebb and spring-neap variations of stratification, mixing and circulation in Chesapeake Bay. Cont. Shelf Res. **29**: 4-14.

Li, M., Y.J. Lee, J.M. Testa, Y. Li, W. Ni, W.M. Kemp and D.M. Di Toro. 2016. What drives interannual variability of hypoxia in Chesapeake Bay: Climate forcing versus nutrient loading? Geophys. Res. Lett**.** **43**: 2127–2134, doi:10.1002/2015GL067334.

Li, M., W. Ni, F. Zhang, P.M. Glibert and C-H. Lin. 2020. Climate-induced interannual variability and projected change of two harmful algal bloom taxa in Chesapeake Bay, U.S.A. Sci. Tot. Environ., doi: 10.1016/j.scitotenv.2020.140947.

Li, Y. and M. Li. 2011. Effects of winds on stratification and circulation in a partially mixed estuary. J. Geophys. Res. **116**: C1202, doi:10.1029/2010JC006893.

McGillicuddy, D.J., D.M. Anderson, D.R. Lynch, and D.W. Townsend. 2003. A mechanism for offshore initiation of harmful algal blooms in the coastal Gulf of Maine. J. Plankt. Res. **25**: 1131–1138.

Montresor M, L. Vitale, D. D'Alelio and M.I. Ferrante. 2016. Sex in marine planktonic diatoms: insights and challenges. Perspect. Phycol. doi.org/10.1127/pip/2016/0045.

Ni, W., M. Li and J.M. Testa. 2020. Discerning effects of warming, sea level rise and nutrient management on long-term hypoxia trend in Chesapeake Bay. Sci. Tot. Environ. doi: 10.1016/j.scitotenv.2020.139717.

North, E.W., Z. Schlag, R. R. Hood, M. Li, L. Zhong, T. Gross and V. S. Kennedy. 2008. Larval vertical swimming behavior may influence the dispersal of oysters in Chesapeake Bay. Mar. Ecol. Prog. Ser. **359**: 99-115.

Shchepetkin, A. F. and J.C. McWilliams. 2005. The regional oceanic modeling system (ROMS): a split-explicit, free-surface, topography-following-coordinate oceanic model. Ocean Model. **9**(4): 347-404.

Stolte, W. and E. Garcés. 2006. Ecological aspects of harmful algal in situ population growth rates. In: E. Granéli and J. Turner [eds.], Ecology of harmful algae. Springer Verlag, Berlin, pp. 139–152.

Suikkanen, S., H. Kaartokallio, S. Hällfors, M. Huttunen and M. Laamanen. (2010) Life cycle strategies of bloom-forming, filamentous cyanobacteria in the Baltic Sea. Deep Sea Res. Part II **57**(3):199–209. doi:10.1016/j.dsr2.2009.09.014.

Tango, P.J., R. Magnien, W. Butler, C. Luckett, M. Luckenbach, R. Lacouture, C. Poukish. 2005. Impacts and potential effects due to *Prorocentrum minimum* blooms in Chesapeake Bay. Harmful Algae **4**: 525–531.

Testa, J.M., Y. Li, Y. Lee, M. Li, D.C. Brady, D.M. DiToro and W.M. Kemp. 2014. Quantifying the effects of nutrient loading and carbon production in dissolved $O_2$ in Chesapeake Bay using a coupled hydrodynamic-biogeochemical model. J. Mar. Syst. **139**: 139-158.

Testa, J.M., Y. Li, Y.J. Lee, M. Li, D.C. Brady, D.M. DiToro, and W.M. Kemp. 2017. Modeling physical and biogeochemical controls on dissolved oxygen in Chesapeake Bay: lessons learned from simple and complex approaches. In D. Justic, K. Rose, R. Hetland, and K. Fennel [eds.], Modeling coastal hypoxia - numerical simulations of patterns, controls and effects of dissolved oxygen dynamics, Springer International Publishing AG, Switzerland, 95-118, doi: 10.1007/978-3-310-54571-4_5.

Tyler, M. A. and H.H. Seliger. 1978. Annual subsurface transport of a red tide dinoflagellate to its bloom area: Water circulation patterns and organism distributions in the Chesapeake Bay 1. Limnol. Oceanogr. **23**(2): 227-246.

Tyler, M. A. and H.H. Seliger. 1981. Selection for a red tide organism: Physiological responses to the physical environment. Limnol. Oceanogr. **26**(2): 310-324.

Xie, X. and M. Li. 2018. Effects of wind straining on estuarine stratification: A combined observational and modelling study. J. Geophys. Res.: Oceans. doi: 10.1002/2017JC013470.

Xie, X., M. Li and W. Ni. 2018. Roles of wind-driven currents and surface waves in sediment resuspension and transport during a tropical storm. J. Geophys. Res.: Oceans. doi: 10.1029/2018JC014104.

Zhang, H. and S. Li. 2010. Effects of physical and biochemical processes on the dissolved oxygen budget for the Pearl River Estuary during summer. J. Mar. Syst. **79**(1-2): 65-88.

Zhong, L. and M. Li. 2006. Tidal energy fluxes and dissipation in the Chesapeake Bay. Cont. Shelf Res. **26**(6): 752-770.

Zhang, F., M. Li, P.M. Glibert, S.H. Ahn. 2021. A three-dimensional mechanistic model for *Prorocentrum minimum* blooms in eutrophic Chesapeake Bay. Sci. Tot. Environ. doi.org/10.1016/j.scitotenv.2020.144528.

Zwiers, F. W. and G.J. Boer. 1987. A comparison of climates simulated by a general circulation model when run in the annual cycle and perpetual modes. Mon. Wea. Rev. **115**(11): 2626-2644.

**Figure Captions**

Figure 1. (a) Map of Chesapeake Bay in which the dashed black line marks the along-channel section in the deep center channel, the filled squares mark the monitoring sites regularly sampled by EPA Chesapeake Bay Program and the black star represents the location used in Fig.4. Color contours indicate depth. (b-f) Along-channel distributions of *Prorocentrum minimum* cell density from the field surveys reported in Tyler and Seliger (1978). Note that contours in (b) and (f) have different units ($10^{-2}$ cells $mL^{-1}$ and cells $mL^{-1}$) from others ($10^{-3}$ cells $mL^{-1}$). Figure reproduced from *Limnol. Oceanog*. with permission of the publisher.

Figure 2. (a)-(h) Time series of the model-predicted surface *P. minimum* cell density at 8 stations arrayed in the along-channel section of Chesapeake Bay (their locations marked in Fig. 1a).

Figure 3. Monthly-mean *P. minimum* cell density in the along-channel section. The vectors are monthly-mean subtidal flow. The color bar is in logarithmic scale and the color scale for (g)-(l) is different from that for (a)-(f) in order to better show the location of *P. minimum* when the cell density is low.

Figure 4. (a) Susquehanna river discharge. (b) Surface-layer (1 m depth, blue) and bottom-layer (15 m depth, red) currents at 150 km from bay's mouth. Positive value indicates landward flow and negative value indicates seaward flow. Dashed red and blue lines are 10-day low passed velocity, and solid lines are monthly averaged velocity.

Figure 5. (a)-(f) Locations of particles released in the bottom water of the lower bay on 1 January, showing how the estuarine return flow transports the particles to the mid-bay to fuel a bloom in May. (g-l) Locations of particles released in the surface water of the mid-bay on 1 July, showing how the estuarine outflow transports the particles to the lower bay during the summer and fall.

Figure 6. Surface distributions of DIN (a), DIP (b), PAR at 2 m depth (c), *P. minimum* cell concentration (d), DIN limitation, DIN limitation (e), DIP limitation, (f) light limitation (g), and *P. minimum* growth rate (h) in May.

Figure 7. Time series of (a) temperature, (b) specific growth rates, (c) growth rate, and (d) biomass of winter-spring diatom group (red), summer dinoflagellate group (green) and *P. minimum* (blue) in the surface water of a mid-bay station CB 4.1C.

Figure 8. Time series of *P. minimum* cell density at CB4.1C obtained from the control model run (a) and the sensitivity-analysis model runs in which the maximum growth rate $G_p$ of *P. minimum* and the shape parameters $\beta_1$ and $\beta_2$ characterizing the window of optimal growth increase or decrease by 20% (b-e).

Figure 9. Schematic diagram of the life strategy of *Prorocentrum minimum.*

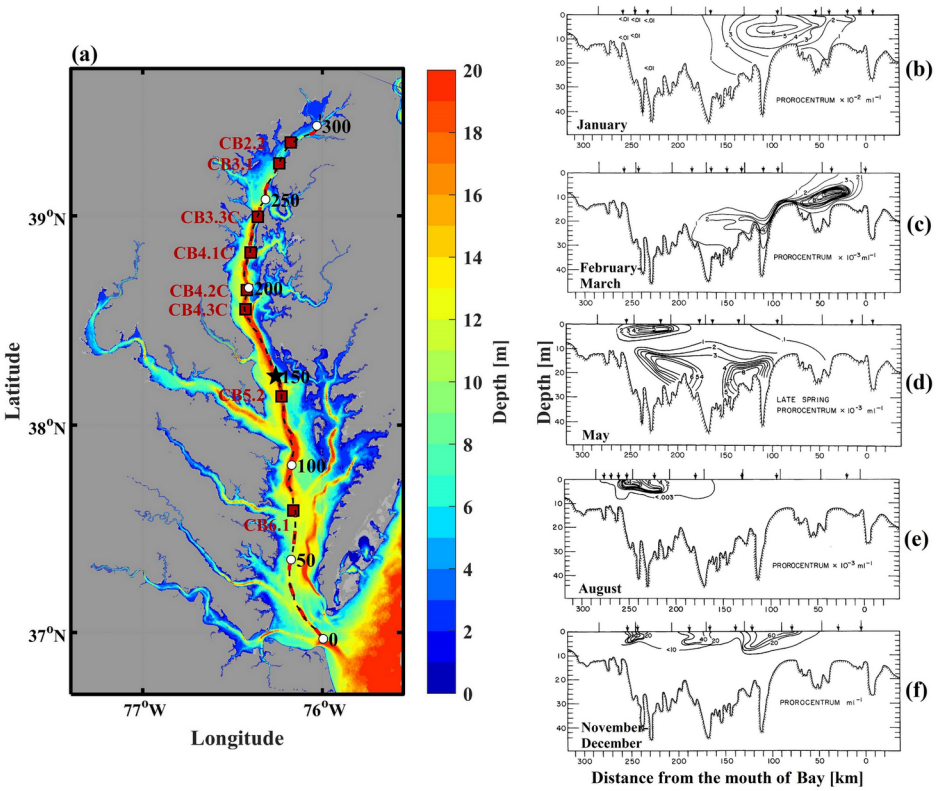


LNO_11925_fig1.tif

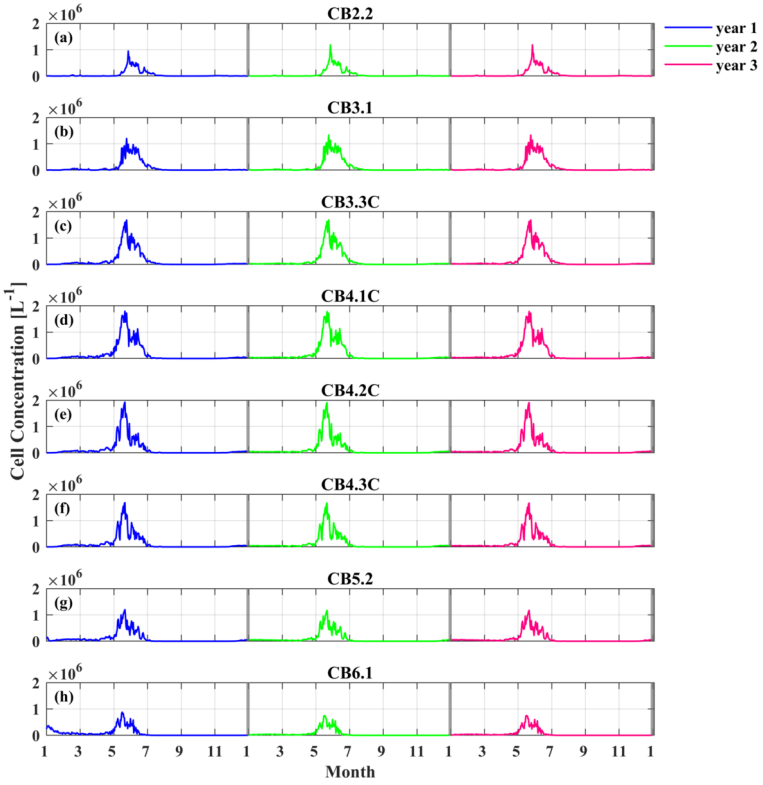


LNO_11925_fig2.tif

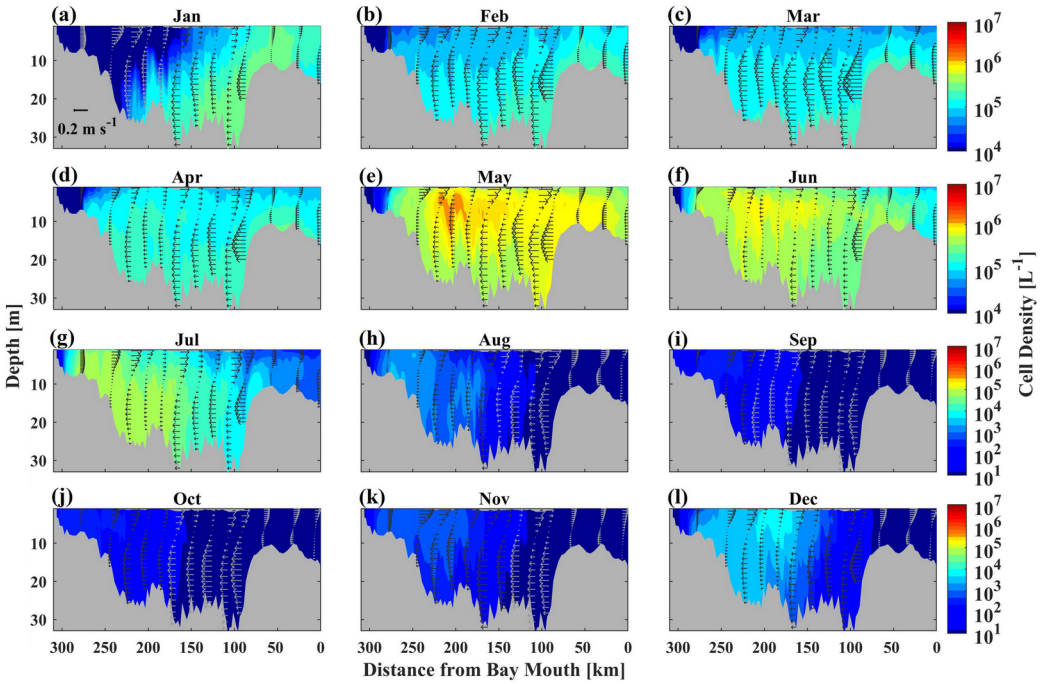


LNO_11925_fig3.tif

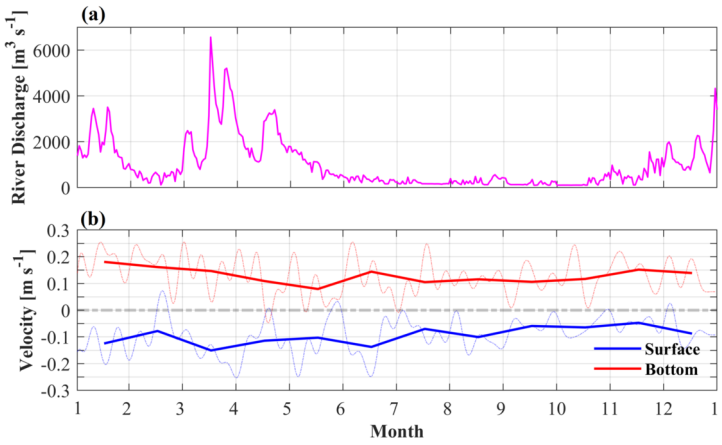


LNO_11925_fig4.tif

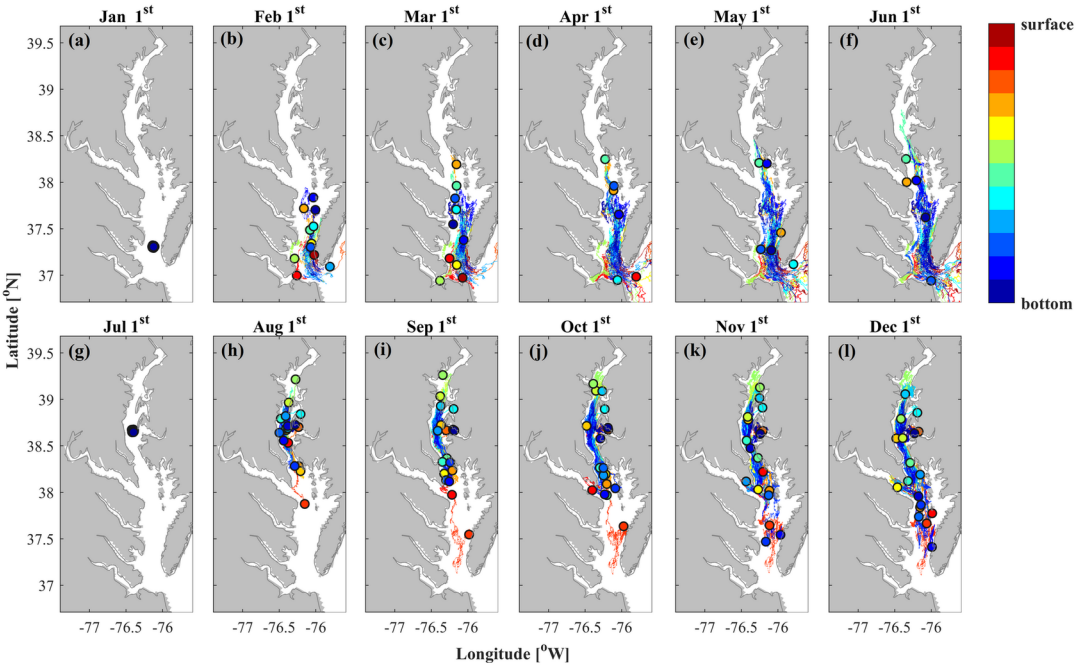


LNO_11925_fig5.tif

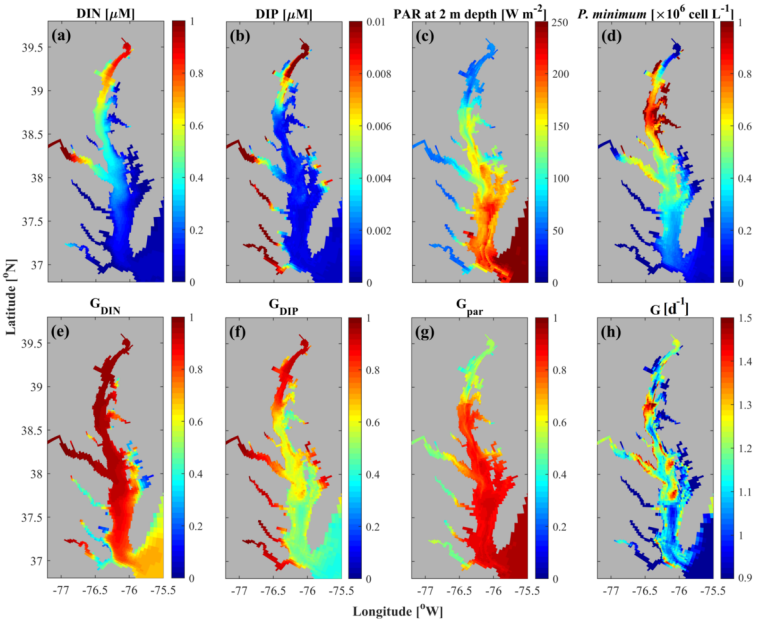


LNO_11925_fig6.tif

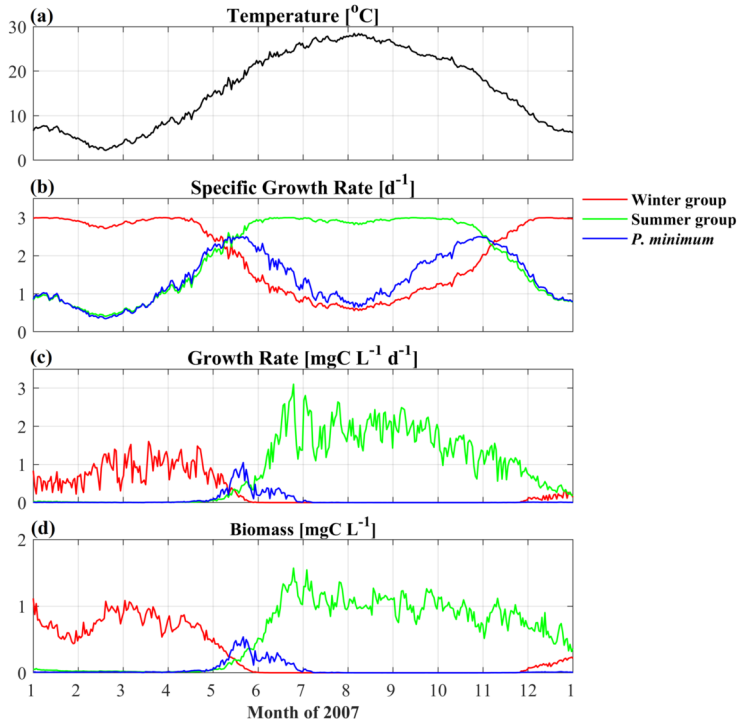


LNO_11925_fig7.tif

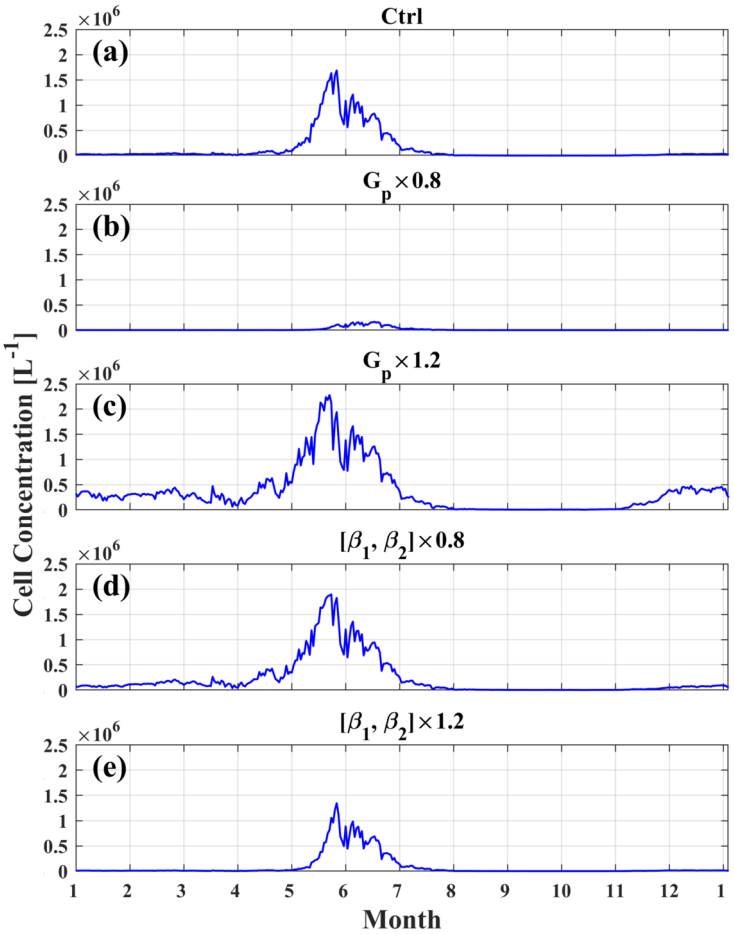


LNO_11925_fig8.tif

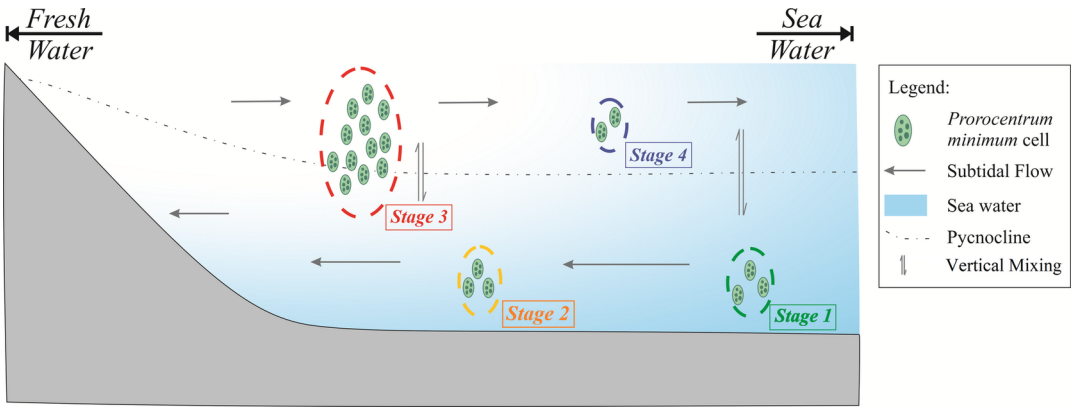


LNO_11925_fig9.tif